Quantum phase transition in NbN superconducting thin films

Tian-Yu Jing,[1] Zi-Yan Han,[1] Zhi-Hao He,[1] Ming-Xin Shao,[2] Peng Li,[2] and Zhi-Qing Li[1,*]

[1]*Tianjin Key Laboratory of Low Dimensional Materials Physics and Preparing Technology, Department of Physics, Tianjin University, Tianjin 300354, China*

[2]*State Key Laboratory of Electronic Thin Films and Integrated Devices, University of Electronic Science and Technology of China, Chengdu 611130, China*

(Received 10 November 2022; revised 27 April 2023; accepted 17 May 2023; published 24 May 2023)

We systematically investigated the low-temperature transport properties of two series of NbN epitaxial films. The first series of films with thickness ranging from ∼2.0 to ∼4.0 nm are two-dimensional (2D) with respect to superconductivity, while another series with thickness around ∼20 nm is quasi-three-dimensional (quasi-3D). Those 2D NbN films undergo a superconductor-insulator transition (SIT) with decreasing film thickness, and the critical sheet resistance for the SIT is close to the quantum resistance of Cooper pairs $h/4e^2$ (6.45 kΩ). Besides the Berezinski-Koterlitz-Thouless transition, a magnetic-field-driven SIT is observed in those 2D superconducting films (2.6 nm $\lesssim t \lesssim$ 4.0 nm). The field-driven quantum metal state does not appear in these 2D superconducting films. However, it is found that both in the 2D and quasi-3D superconducting films the low-temperature magnetoresistance isotherms do not cross at a very narrow region (generally treated as a single point) but cross at a well-distinguished wide region. The dynamical critical exponent obtained by analyzing these magnetoresistance isotherms is divergent as the quantum critical point is approached. The divergence of the dynamical critical exponent near the critical point is consistent with the quantum Griffiths singularity behavior. Our results suggest that the quantum Griffiths singularity can also occur in a 2D superconductor with SIT or a quasi-3D superconductor. The origin of the infinite-randomness point of the quantum phase transition is attributed to the emergence of superconducting rare regions due to the quench disorder in low temperatures.

DOI: 10.1103/PhysRevB.107.184515

I. INTRODUCTION

Two-dimensional (2D) superconductors are good systems for investigating quantum phase transition and have attracted great attention over the past decades. The superconductor-insulator/metal transition (SIT/SMT) in 2D superconductors is a typical quantum phase transition and can be tuned by magnetic field [1,2], carrier concentration [3], or degree of disorder [4,5]. Generally, the SIT in 2D homogeneous superconductors is explained in the framework of "dirty-boson model", which predicts that the ground state of the system directly changes from superconducting to insulating states without passing through an intermediate metal regime. In addition, this model predicts that a magnetic field would induce a SIT, in which the sheet resistance of the superconducting film satisfies a power-law scaling form [6,7]

$$R_\square(B, T) = R_\square^c f(\delta T^{-1/\nu z}), \quad (1)$$

where $\delta = |B - B_c|$ is the distance from the critical field B_c, $R_\square^c$ is the critical sheet resistance, ν is the correlation length exponent, z is the dynamical critical exponent, and $f(x)$ is the scaling function with $f(0) = 1$. Experimentally, the values of $z\nu$ were found to be ≈0.65 [8,9], ≈1.33 [2,10], and ≈2.33 [11,12], respectively. With the assumption $z = 1$, $\nu = 2/3$ and 4/3 (7/3) would correspond to the universality class of $(2+1)$D XY model [13] and classic (quantum) percolation model for SIT [11], respectively. The scaling form in Eq. (1) implies that the magnetic field dependence of resistance curves at different temperatures all cross at the critical field B_c. Since 1996, the experimental results have indicated that an intermediate anomalous metallic state appears in some 2D superconductors, including amorphous $Mo_{43}Ge_{57}$ [14] and Ta thin films [15], ZrNCl-based electric-double layer transistors [3], mechanically exfoliated crystalline $NbSe_2$ [16] and WTe_2 films [17], and Josephson junction arrays [18,19]. Recently, it has been found that in some 2D superconductors the magnetoresistance isotherms do not cross at a fixed point or a narrow region near the critical field but at multiple points, and the effective exponent $z\nu$ determined at each crossing point diverges as the quantum phase transition is approached [20–26]. This phenomenon is the so-called quantum Griffiths singularity (QGS). The appearance of QGS in 2D superconductors does not conform to the "dirty-boson model" either.

The QGS was initially observed in 3-monolayer Ga film [20], and subsequently observed in some crystalline 2D superconductors, such as $LaAlO_3/SrTiO_3$ interface [21], macrosize monolayer $NbSe_2$ [22], and ion-gated ZrNCl and MoS_2 [23]. The QGS has also been observed in amorphous InO_x [24], WSi [25], and β-W [26] films. In addition, the QGS was found in a graphene/Pb-islands-array hybrid (an artificial 2D superconductor system) [27]. The QGS phase in the films (or devices) mentioned above is induced by a perpendicular magnetic field (out-of-plane). Recently, it was reported that

*Corresponding author: zhiqingli@tju.edu.cn

the QGS can be induced by both perpendicular and parallel magnetic field in four-monolayer crystalline $PdTe_2$ films [28]. It is believed that quenched disorder plays an important role for the occurrence of QGS in the 2D superconductors [20–23]. According to previous reports [20–23], those 2D superconductors with QGS are gradually changed from a superconducting state to a metal or weakly localized-metal state when the applied magnetic field is gradually increased, i.e., the QGS mainly emerges in 2D superconductors with SMT. Therefore, it is necessary to explore whether there is QGS in crystalline 2D superconducting film with SIT. In addition, it is interesting to check whether the QGS could present in quasi-three-dimensional or three-dimensional (3D) samples.

The NbN superconductor films could be a suitable system to address the above issues. There are several advantages for using NbN films. (1) The superconducting transition temperature of NbN film can still be as high as 9 K even if the film thickness is only 3 nm [29]. (2) A NbN film possesses high resistance to oxidation at room temperature. (3) It has been demonstrated that superconducting puddles (or islands) appear in the NbN film below T_c [30–33], which could be a necessary condition for the occurrence of QGS in 2D superconductors. In the present paper, we systematically investigate the electrical transport properties of a series of 2D (with respect to superconductivity) and two quasi-3D NbN films. For the 2D superconducting films, the magnetic-field-induced SIT as well as the QGS is observed. The QGS state is also observed in the quasi-3D films. We will report these interesting phenomena in the following sections.

II. EXPERIMENTAL METHOD

Our NbN films with thickness ranging from ~2.0 to ~100 nm were grown on (100) MgO single crystal substrates by the standard reactive magnetron sputtering method. A commercial niobium target with purity of 99.99% was used as the sputtering source. The base pressure of the chamber was less than 1×10^{-5} Pa. The deposition was carried out in a mixture of argon (99.999%) and nitrogen (99.999%) atmosphere and the pressure of the chamber (working pressure) was kept at 0.2 Pa. During the deposition, the sputtering power was set as 300 W. It was found that the optimal substrate temperature and volume ratio of nitrogen to argon were 763 K and 1 : 15 (the percentage of nitrogen is 6.25%), respectively. When the thickness of the film is fixed, the NbN film deposited at the optimal conditions has the highest superconducting transition temperature (T_c) and highest upper critical field (at a certain temperature). The superconducting transition temperature and the upper critical field (at a fixed temperature) increase rapidly with increasing film thickness t, meanwhile both of them can be reduced by increasing the nitrogen partial pressure. In this paper, the superconductor to insulator (or metal) transition is mainly obtained via the magnetoresistance measurement, which requires the applied field to be much larger than the upper critical field of the film. Thus, the 2D films ($t \lesssim 4.0$ nm) used for investigating the quantum phase transition are deposited at the optimal conditions. While for the thicker films (~20 nm) used for investigating the quantum phase transition, the volume ratio of nitrogen to argon is increased to 1 to 7 and 3 to 17 (the corresponding percentages of nitrogen are 12.5% and 15%, respectively).

The thicknesses of the films were evaluated through growth rate and deposition time: fixing the deposition conditions, including sputtering power, substrate temperature, ratio of nitrogen to argon, and working pressure, we first fabricated some thick films ($t > 200$ nm); the thicknesses of these thick films were measured using a surface profiler (Dektak, 6M), and then the growth rate was obtained. The thicknesses of the $t \lesssim 20$ nm films were further determined by the high resolution transmission electron microscopy (HRTEM) of the cross section of the films. Crystal structure and phase characterization were determined by x-ray diffraction (XRD) with Cu K_α radiation at room temperature. The microstructure of the films was characterized by transmission electron microscopy (TEM, Tecnai G2 F20 S-Twin). The isothermal current-voltage (I-V) curves and the resistance versus temperature and magnetic field (being perpendicular to the film planes for all the tested films) were measured using the standard four-probe method in a physical property measurement system (PPMS-6000, Quantum Design) equipped with a ^{3}He refrigerator. A Keithley 2400 Source Measure Unit was used to measure the I-V curves. Hall-bar-shaped films (1.0-mm wide and 10.0-mm long, and the distance between the two voltage electrodes is 3 mm), defined by mechanical masks, were fabricated for the resistance and I-V curve measurements. To obtain good contact, four Ti/Au electrodes were deposited on the films.

III. RESULTS AND DISCUSSIONS

A. Crystal structure and morphologies

Figure 1(a) shows the XRD θ-2θ scan profiles for four NbN films with different thickness and deposited at the optimal condition. Besides the (200) diffraction peak of the MgO substrate, only the peak related to the (200) plane of δ-NbN (Rocksalt structure) appears in each XRD pattern. Thus, δ-NbN films without any impurity phase are successfully fabricated at the optimal the conditions. The full width at half maximum of the (200) peak increases with decreasing film thickness, while the intensity of the peak decreases with decreasing thickness. When the thickness of the films is less than ~10 nm, the diffraction intensity of the film is too weak to be observed. Figure 1(b) shows the ϕ-scan profile of (220) plane of the 50-nm film (the ϕ-scan profiles of those $t \gtrsim 30$ nm films are similar). Clearly, four uniformly distributed diffraction peaks appear in the profile, indicating that the NbN film is epitaxially grown on the MgO substrate. For the films deposited at higher nitrogen partial pressures (12.5% and 15%), the XRD patterns [Figs. 1(c) and 1(d)], including θ-2θ and ϕ scans, are similar to those for films deposited at the optimal conditions. The values of the lattice constant a, evaluated from the (200) diffractions of the ~50-nm-thick films, decrease with increasing nitrogen partial pressures. For the films deposited at the optimal conditions, 12.5%, and 15% nitrogen partial pressures, the values of a are 0.444, 0.439, and 0.435 nm, respectively. In addition, for the ~50-nm-thick films deposited at different nitrogen partial pressures, the full width at half maxima increases with increasing the nitrogen partial pressure [see the insets of Figs. 1(b) and 1(d)].

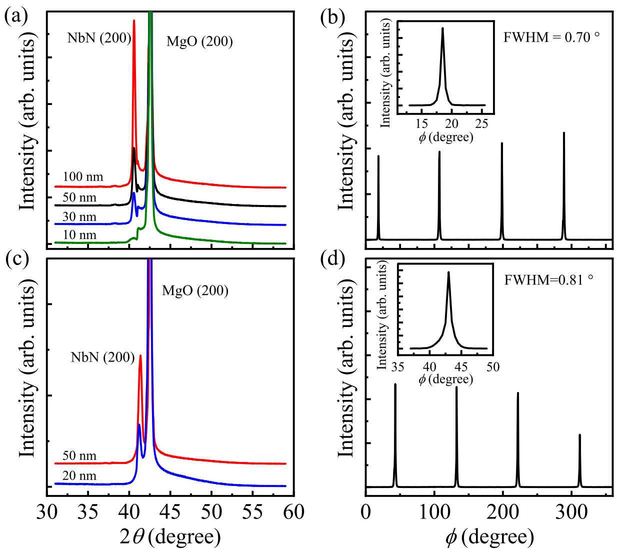

FIG. 1. (a) XRD θ-2θ scan patterns of NbN films with different thickness deposited under the optimal conditions. (b) ϕ-scan spectrum of (220) plane for the 50-nm-thick NbN film deposited under the optimal conditions. (c) XRD θ-2θ scan patterns of the 20- and 50-nm-thick NbN films deposited at the atmosphere with 12.5% nitrogen. (d) ϕ-scan spectrum of (220) plane for the 50-nm-thick NbN film deposited at the atmosphere with 12.5% nitrogen. The insets in (b) and (d) are the enlarged views of the peaks located at the minimum ϕ angles for the corresponding films.

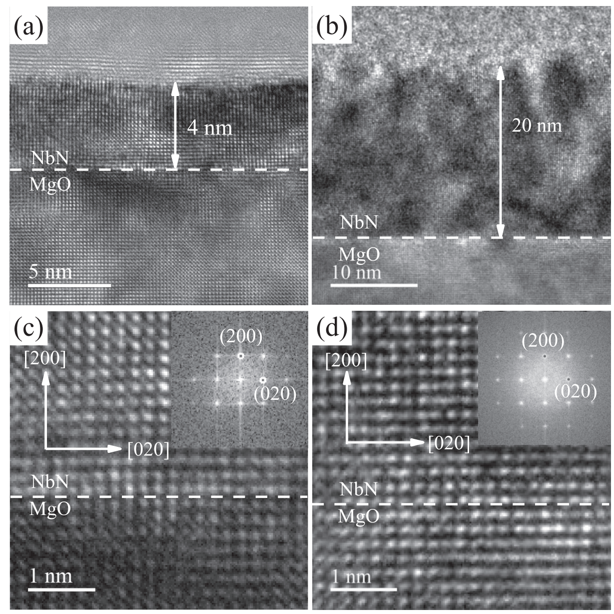

FIG. 2. Cross-sectional HRTEM micrographs of (a) the 4.0-nm-thick film deposited at the optimal conditions and (b) the 20-nm-thick film deposited at the atmosphere with 12.5% nitrogen. (c) and (d) are the enlarged images near NbN/MgO interface for the two films, respectively. The insets in (c) and (d) are the Fourier transforms of the HRTEM images of NbN regions for the corresponding films.

For the $t \lesssim 20\,\mathrm{nm}$ films, we use the TEM to further detect their structures and morphologies. Figures 2(a) and 2(b) shows the cross-sectional HRTEM micrographs of a $\sim$4.0-nm-thick film (deposited at the optimal conditions) and a $\sim$20-nm-thick film (deposited at atmosphere with 12.5% nitrogen) along the [001] axis, respectively. The NbN/MgO interface and the surface of NbN film can be clearly identified and the average thickness of each film can be obtained [see Figs. 2(a) and 2(b)]. It is found that the thickness of each film obtained from TEM measurement is almost identical to that evaluated via growth rate and deposition time. Figures 2(c) and 2(d) present the enlarged HRTEM images near the interface of NbN film and MgO substrate for the $\sim$4.0 nm and $\sim$20 nm films, respectively. Combining the XRD result for the thick NbN films, one can readily obtain that the [200]-orientated δ-NbN film is epitaxially grown on the (100) MgO substrate. The insets of Figs. 2(c) and 2(d) are the fast Fourier transform images of the NbN films, which further confirm the epitaxial characteristics of the δ-NbN films. We note in passing that the NbN film is still uniform and completely covers the MgO substrate even if the film is only as thin as $\sim$2.0 nm.

B. The fundamental transport properties

Figure 3(a) shows the sheet resistance $R_\square$ as a function of temperature for the NbN films with different thickness deposited at the optimal conditions. Clearly, those $t \gtrsim 2.6$ nm NbN films reveal superconductor characteristics at low temperature regime, while those $t \lesssim 2.4$ nm films exhibit insulator behaviors, i.e., $dR_\square/dT < 0$ over the whole measuring temperature range and $d\ln\sigma_\square/d\ln T \to \infty$ as $T \to 0$ [see Fig. 3(b), here the sheet conductance $\sigma_\square$ is the reciprocal of $R_\square$]. It is worth noting that the behavior of the logarithmic derivative of the sheet conductance $w = d\ln\sigma_\square/d\ln T$ near 0 K is more reliable than the behavior of the derivative of the sheet resistance $dR_\square/dT$ in determining whether a certain sample is metallic or insulating [34]. For the metallic sample, the value of w tends to be zero as $T \to 0$, while w tends to be a constant or divergent value as $T \to 0$ for the insulating sample. From Fig. 3(a), one can also see that the NbN films directly change from superconductors to insulators at low temperature with decreasing thickness and the transition (intermediate) states that often appear in granular films, such as

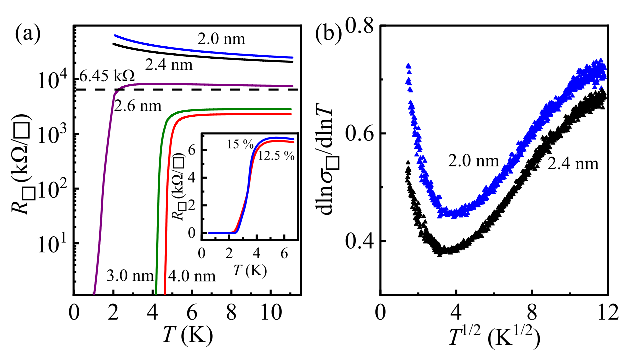

FIG. 3. (a) Sheet resistance $R_\square$ as a function of temperature T for the NbN films with different thickness. Inset: $R_\square$ vs T for the 20-nm-thick NbN films deposited at the atmosphere with 12.5% and 15% nitrogen. (b) $d\ln\sigma_\square/d\ln T$ versus $T^{1/2}$ for the 2.4 and 2.0 nm NbN films.

TABLE I. Relevant parameters for the NbN films with different thickness t. Here $R_\square^{\rm N}$ is normal state sheet resistance at 10 K, T_c is the superconducting transition temperature, $\xi(0)$ is the coherence length at 0 K, $T_{\rm BKT}$ is BKT transition temperature, R_0 and b are the parameters in Halperin-Nelson formula, C is the parameter in the activated scaling law (See the text), B_c^* is the characteristic critical field, and $T_{\rm M}$ is vortex melting temperature. Films No. 1, No. 2, and No. 3 are deposited at the optimal conditions, while films No. 4 and No. 5 are deposited at the atmospheres with 12.5% and 15% nitrogen, respectively.

Film No.	t (nm)	$R_\square^{\rm N}$ (k$\Omega/\square$)	T_c (K)	$\xi(0)$ (nm)	$T_{\rm BKT}$ (K)	R_0 ($\Omega/\square$)	b	C	B_c^* (T)	$T_{\rm M}$ (K)
1	2.6	7.59	2.38	10.09	1.43	27116	1.09	0.29	3.87	0.8
2	3.0	2.84	5.47	6.96	4.13	11125	0.62	0.34	5.83	0.9
3	4.0	2.31	5.79	6.63	4.59	13480	0.71	0.40	8.58	1.2
4	20	6.00	3.80	5.95	–	–	–	0.35	9.82	1.0
5	20	6.21	3.69	6.20	–	–	–	0.31	9.08	0.8

"quasireentrant" behavior or "flat tail" of the low-temperature resistance [35], are not present. In addition, the critical sheet resistance $R_\square^{\rm c}$ [the sheet resistance at normal state (10 K)] for the SIT is very close to the quantum resistance of Cooper pairs $h/4e^2$ or 6.45 kΩ. According to Fisher *et al.* [36], the critical sheet resistance for SIT in disordered 2D superconducting systems is universal, being close to the quantum resistance of Cooper pairs $h/4e^2$. The inset of Fig. 3(a) shows the temperature dependence of the sheet resistance for the two 20-nm-thick films deposited at higher nitrogen pressures. The relation between the resistivity ρ and sheet resistance $R_\square$ is $\rho = R_\square t$. For consistency, we still use the sheet resistance to express the conductive ability of the 20-nm-thick films. For the 20-nm-thick film deposited at the optimal conditions, the sheet resistance and superconducting transition temperature are 458.59 $\Omega/\square$ and 10.65 K, respectively. While the sheet resistances are enhanced and the superconducting transition temperatures are significantly suppressed by increasing the nitrogen partial pressure. It is also found that the upper critical field of NbN film is also greatly reduced via the enhancement of the nitrogen partial pressure (see further remarks in the next subsection).

The coherence lengths $\xi(0)$ of the films can be evaluated via $\xi(0) = [\Phi_0/(2\pi B_{c2}(0))]^{1/2}$, where Φ_0 is the flux quantum and $B_{c2}(0)$ is the upper critical field at 0 K. For our NbN films, the value of $B_{c2}(0)$ is determined by least-square fitting the $T_c(B)$ data to $B_{c2}(T) = B_{c2}(0)[1-(T/T_c)^2]$, where T_c is the superconducting transition temperature at which the resistance drops to 90% of the normal-state resistance. In Table I, we give the calculated value of $\xi(0)$ for each film. The coherence lengths of the films lie between ∼6.0 and 10.0 nm, which is consistent with those in previous reports [37,38] Thus, those NbN films with $2.6 \lesssim t \lesssim 4.0$ nm are 2D with respect to superconductivity, while the two ∼20- nm-thick films are quasi-3D.

A 2D superconductor with high normal state sheet resistance and lateral size of order of the transverse penetration depth $\lambda_\perp$ [$\lambda_\perp = \lambda^2(T)/d$ with $\lambda(T)$ being the usual bulk magnetic penetration depth] is expected to exhibit the Berezinskii-Kosterlitz-Thouless (BKT) transition [39–42]. Below the BKT transition temperature $T_{\rm BKT}$ (which is somewhat less than the thermodynamic superconducting transition temperature T_c), the vortices are bound in vortex-antivortex pairs. In each vortices pair, the helicities of the two vortices are opposite, and the separation (distance) between the two vortices is less than $\lambda_\perp$. Above $T_{\rm BKT}$, the pairs are thermally dissociated and the motion of the dissociated vortex pairs should lead to a broadened superconducting transition.

Experimentally, the occurrence of BKT transition can be identified by analyzing the variations of the characteristic physical quantities near $T_{\rm BKT}$, such as, the temperature dependence of sheet resistance [43,44], the current-voltage curves [45], the rf surface impedance [46], and the voltage noise spectra [47]. For a 2D superconductor with BKT transition, the temperature dependent behavior of the sheet resistance can be described by the Halperin-Nelson formula [48]

$$R_\square = R_0 \exp[-b(T/T_{\rm BKT}-1)^{-1/2}] \qquad (2)$$

as the transition temperature $T_{\rm BKT}$ is approached from above. Here both R_0 and b are constants. Figure 4(a) shows the temperature dependence of the sheet resistance at low temperature regime for two representative films (the 3.0- and 4.0-nm-thick films). The solid curves are the least-squares fits to Eq. (2). In the fitting process, R_0 and b are the adjustable parameters, and $T_{\rm BKT}$ is obtained by extrapolating the linear part of $({\rm d}\ln R_\square/{\rm d}T)^{-2/3}$ vs T curve to $({\rm d}\ln R_\square/{\rm d}T)^{-2/3}=0$. Clearly, the $R_\square(T)$ data of the two films near the transition regions can be well described by Eq. (2). For the $2.6 \lesssim t \lesssim 4.0$ films, the adjusting parameters R_0 and b, as well as the value of $T_{\rm BKT}$, are listed in Table I. Inspection of the table indicates that the values of b for the four samples are all around 1, which is consistent with the theoretical predication [48]. Figure 4(b)

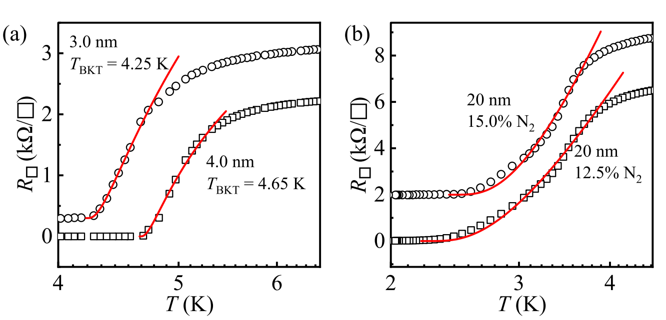

FIG. 4. The sheet resistance $R_\square$ vs temperature T for (a) the 3.0- and 4.0-nm-thick films deposited at the optimal conditions, and (b) the 20-nm-thick films deposited at atmospheres with 12.5% and 15% N_2. The solid curve is the least-squares fit to Eq. (2). For clarity, the data for the 3.0-nm-thick film and film deposited at 15% N_2 have been shifted by +0.3 kΩ and +2.0 kΩ, respectively.

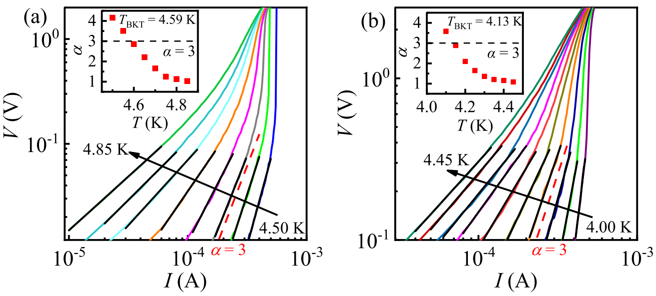

FIG. 5. Voltage vs current (double logarithmic scales) measured at fixed temperatures at zero magnetic field for the (a) 4.0-nm-thick and (b) 3.0-nm-thick films. The temperature difference between two adjacent curves is 0.05 K. The solid black lines are least-squares fits to $V \sim I^{\alpha(T)}$, and the dashed line represents the line with $\alpha = 3$. Inset: the exponent α vs temperature for the two films.

shows the temperature dependence of the sheet resistance at low temperature regime for the ∼20-nm-thick films deposited at 12.5% and 15% nitrogen partial pressures. These data in the superconducting transition regions are also least-squares fitted to Eq. (2) (solid curves). The experimental data obviously deviate from the theoretical predictions of Eq. (2), suggesting that the BKT transition does not emerge in the two quasi-3D NbN films.

As mentioned above, the occurrence of BKT transition can also be evaluated via the measurements of *I*-*V* curves around the transition region. For the 2D superconductor with BKT transition, Kadin *et al.* [49], have demonstrated that in the transition regime and in the limit of arbitrarily small current, the current dependence of voltage obeys $V \sim I^{\alpha(T)}$, where $\alpha(T)$ is a measure of the areal superelectron density and $\alpha(T) = 3$ at $T_{\rm BKT}$. In Figs. 5(a) and 5(b), we present the isothermal *I*-*V* curves for two representative films, respectively, as indicated. Clearly, $\log_{10} V$ varies linearly with $\log_{10} I$ in small current limit at each selected temperature, which means that the voltage variation with the current obeys the power law ($V \sim I^{\alpha}$) for each sample. The temperature dependence of α is given in the insets of Figs. 5(a) and 5(b). Clearly, the value of α decreases with increasing temperature, and the temperatures for $\alpha = 3$ are ∼4.59 K and ∼4.13 K, respectively, for the $t \simeq 4.0$ and 3.0 nm films. The values of $T_{\rm BKT}$ are almost identical to those determined by the Halperin-Nelson formula. Thus, the occurrence of BKT transition in the films is confirmed. The above results further indicate that these $2.6 \lesssim t \lesssim 4.0$ nm NbN films are 2D with respect to the superconductivity.

C. Quantum phase transition

Firstly, we discuss the quantum phase transition in those 2D ($2.6 \lesssim t \lesssim 4.0$ nm) films. Considering the quantum phase transition can be induced by an external magnetic field, we measured the temperature dependence of $R_\square$ under different fields for the $t \simeq 4.0$, 3.0, and 2.6 nm films. Since the results of the three films are similar, we only give and discuss those obtained from the $t \simeq 4.0$ film. Figure 6(a) shows $R_\square$ as a function of T from 10 to 0.5 K under different fields. For $B \lesssim 5.0$ T, the film is in superconducting state at low temperature. As the field is increased to 9.0 T, the film converts

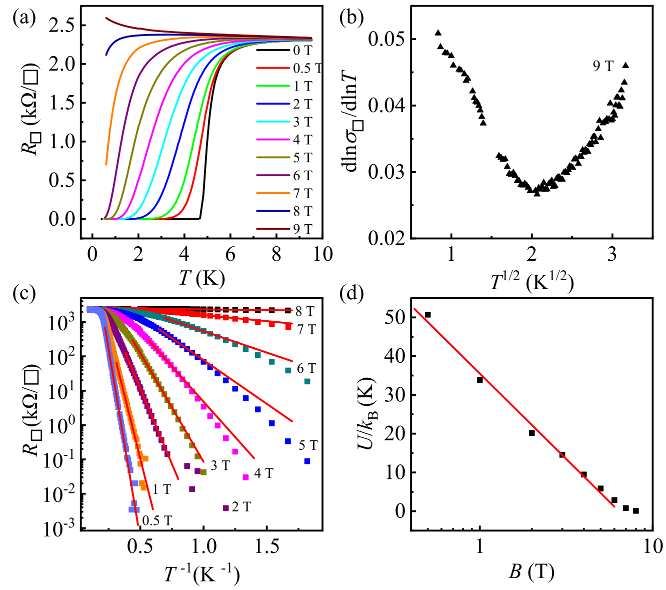

FIG. 6. (a) $R_\square(T)$ as a function of temperature for the 4.0-nm-thick NbN film measured at different fields perpendicular to the film plane. (b) $d\ln\sigma_\square/d\ln T$ vs $T^{1/2}$ for the 4.0-nm-thick NbN film under 9 T. (c) Logarithm of the sheet resistance as a function of T^{-1} at different magnetic fields for the 4.0-nm-thick film. The symbols are the experimental data and the straight solid lines are least-squares fits to Eq. (3). (d) Activation energy $U(B)/k_{\rm B}$, obtained from the slopes of the solid lines in (c), as a function of magnetic field. The solid line is the least-squares fit to $U(B) = U_0 \ln(B_0/B)$.

into an insulator. Here the insulator still refers to the sample with $dR_\square/dT < 0$ and $d\ln\sigma_\square/d\ln T|_{T\to 0} \to \infty$ or constant [see Fig. 6(b)]. The critical field of SIT lies between 8 and 9 T. To check whether there is intermediate metal state in the film, the $R_\square(T)$ data in Fig. 6(a) are redrawn as $R_\square$ (in logarithmic scale) versus T^{-1}, shown in Fig. 6(c). Upon cooling, the film directly changes from normal to superconducting states as the external field is less than ∼5 T. When the applied field is between ∼5 and ∼7 T, the sheet resistance drops sharply below $T_c(B)$, where $T_c(B)$ is designated as the temperature at which the resistance drops to 90% of the normal state resistance $R_\square^{\rm N}$ under B. The saturation trend appearing in the 2D superconductors with field-driven anomalous metal state was not observed. Inspection of Fig. 6(c) also indicates that the $\log_{10} R_\square$ (or $\ln R_\square$) varies linearly with T^{-1} below $T_c(B)$. Thus, the sheet resistance can be described by

$$R_\square = R_0(B)\exp[-U(B)/k_{\rm B}T] \tag{3}$$

around the transition region, where $R_0(B)$ is a prefactor, $k_{\rm B}$ is the Boltzman constant, and $U(B)$ is the activation energy under B. This means that the vortex-antivortex pairs are thermally dissociated into vortices and the motion of thermally activated individual vortices dominates the charge transport process in the transition region. The experimental $R_\square(T)$ data at a certain B are least-squares fitted to Eq. (3) and the results are shown as the solid lines in Fig. 6(c). Thus, the activation energy $U(B)$ as a function of B can be obtained and is shown in Fig. 6(d). Clearly, $U(B)$ varies linearly with $\log_{10}(1/B)$ ($\ln(1/B)$), i.e., $U(B)$ vs B satisfies $U(B) = U_0 \ln(B_0/B)$, which is in accordance with the theoret-

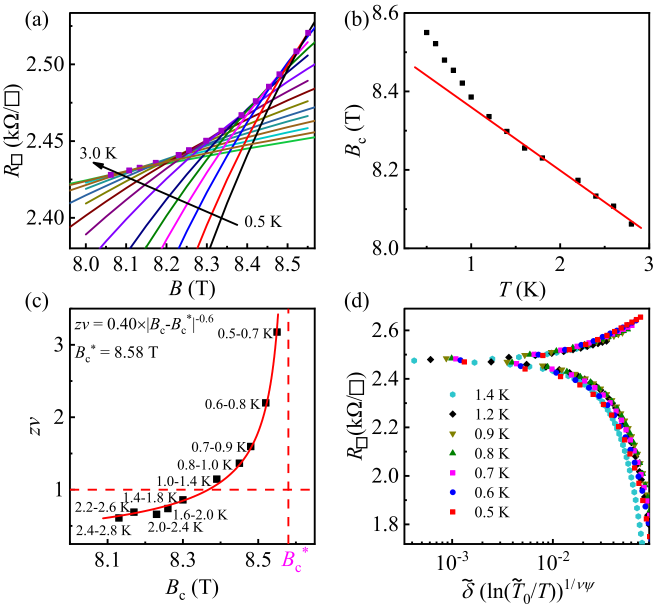

FIG. 7. (a) The sheet resistance vs magnetic field at different temperature for the 4.0-nm-thick NbN film. The temperature interval between two adjacent curves is 0.10 K from 0.50 to 1.00 K, while the interval is 0.20 K from 1.00 to 3.00 K. (b) Temperature dependence of crossing points (denoted as B_c) of $R_\square(B)$ at every two adjacent temperature. The solid line is only the guide for eyes. (c) The critical field B_c dependence of critical exponent $z\nu$. (d) Sheet resistance vs the scaling parameter described in Eq. (4) for activated scaling.

ical predication of thermally assisted collective vortex-creep model for 2D superconductor [50].

As mentioned in Sec. I, the "dirty-boson model" predicts that the $R_\square$ vs B curves at different temperatures all cross at the critical field B_c. To check whether this model is suitable for the 2D NbN films, the magnetoresistance isotherms at temperatures from 0.5 to 3 K have been measured and are shown in Fig. 7(a). Clearly, these $R_\square$-B curves do not cross at one point or a narrow region, but the crossing points of two adjacent isotherms form a continuous curve over a wide range of temperatures and magnetic fields. This unusual phenomenon is very similar to that in three-monolayer Ga films [20] and is the signature of the QGS. Designating the magnetic field at each crossing point as the critical field B_c, one can readily obtain the critical field variation with temperature, which is shown in Fig. 7(b). Upon cooling, the critical field almost increases linearly with decreasing temperature from 3 to ∼1.2 K, and then increases more rapidly below ∼1.2 K. Assuming the $R_\square$-B curves measured at three adjacent temperatures cross at one point, we rewrite Eq. (1) as $R_\square(B,\tilde{t}) = R_\square^c f[(B-B_c)\tilde{t}]$ [with $\tilde{t} = (T/T_0)^{-1/z\nu}$ and T_0 being the lowest temperature] and use the equation to analyze the magnetoresistance isotherms. It is found that the $R_\square(B,T)$ data for the three adjacent temperatures collapse onto two branches in the $R_\square(B,T)$ vs $\delta\tilde{t}$ plot as a suitable $\tilde{t}$ is selected. Thus the effective critical exponent $z\nu$ at a certain temperature range can be obtained, and $z\nu$ vs B_c for the 4-nm-thick film is summarized in Fig. 6(c). In the high temperature regime ($T \gtrsim 1.2$ K), the effective critical exponent $z\nu$ increases slowly with increasing B_c, then increases dramatically in the low temperature regime, and finally tends to diverge as $B_c \to B_c^*$, where B_c^* is a characteristic field. The behavior of $z\nu$ is quite different to that of the conventional SIT in highly and homogeneously disordered 2D superconductors, in which $z\nu$ keeps as a constant in the vicinity of the transition. The $z\nu$ vs B_c data are least-squares fitted to the activated scaling law [51] $z\nu = C|B_c - B_c^*|^{-\nu\psi}$ with C being a constant, the correlation length exponent $\nu = 1.2$, and the tunneling exponent $\psi = 0.5$, and the fitting result is shown by the solid curve in Fig. 7(c). Clearly, the experimental $z\nu$ vs B_c data can be well described by the activated scaling law with $B_c^* \approx 8.58$ T, which is the evidence of QGS associates with an infinite-randomness critical point.

In fact, Maestro *et al.* [52] have proposed an activated scaling law theoretically to describe the conductivity of the quantum Griffiths phase of disordered nanowires. The scaling theory has also been extended to the quantum phase transition in higher dimensions. Recently, it has been found that the scaling law can be used to analyze the magnetoresistance isotherms of 2D disordered amorphous indium oxide films near the quantum critical point [24]. According to Maestro *et al.* [52] and Lewellyn*et al.* [24], for films with infinite-randomness fixed point of the quantum SMT, the sheet resistance vs magnetic field at different temperatures is described by

$$R_\square\left(\tilde{\delta}, \ln\frac{\tilde{T}_0}{T}\right) = \Phi\left[\tilde{\delta}\left(\ln\frac{\tilde{T}_0}{T}\right)^{1/\nu\psi}\right], \tag{4}$$

where $\tilde{\delta} = |B - B_{c0}|/B_{c0}$ with B_{c0} being the critical field, and $\tilde{T}_0$ is a characteristic temperature. Taking $\nu\psi = 0.60$, we check whether the low-temperature $R_\square(T,B)$ data can be described by Eq. (4). Fixing B at a certain value of B_c shown in Fig. 7(b), we first get the critical field B_{c0} via minimizing the variance $\sum_{i=1}^{n-1} |R_\square(T_i,B) - R_\square(T_{i+1},B)|^2$, where T_i is a testing temperature. The obtained value of B_{c0} is 8.44 T, which is 1.6% less than the value of B_c^*. Then $\tilde{T}_0$ is set as an adjustable parameter, and it is found that the $R_\square(T,B)$ vs $\tilde{\delta}[\ln(\tilde{T}_0/T)]^{1/\nu\psi}$ data almost collapse onto two branches as $\tilde{T}_0 \approx 1.67$ K. Thus the $R_\square(T,B)$ data obey the activated dynamical scaling law [Eq. (4)], which strongly suggests that the quantum superconductor-insulator transition in 2D NbN film is governed by an infinite-randomness fixed point with activated dynamical scaling from the other side. Inspection of Fig. 7(d) indicates that the $R_\square(T,B)$ data deviate from the scaling law for both the upper and low branches when the values of the scaling parameter (the value of the abscissa) is larger than ∼0.013. In this region, the upper branch corresponds to the field being higher than ∼8.6 T, while the low branch corresponds to the field being less than ∼8.3 T. In the high field (low field) case, the film has left the quantum critical regime and the influence of the quantum fluctuation on the properties of the film is negligibly weak, which causes the $R_\square(T,B)$ data to deviate from the scaling rule of Eq. (4) in the high scaling parameter regime.

Theoretically, the origin of the QGS is the quenched disorder [51,52]. In an epitaxial NbN film, the quenched disorder is mainly caused by the intrinsic defects, such as dislocations, nitrogen or Nb vacancies. At low temperatures, the phase diagram of the epitaxial NbN film is determined by the interplay of the quantum fluctuation, quenched disorder, and thermal fluctuation. As mentioned above, the critical field B_c increases abruptly below ∼1.2 K. Inspection of Fig. 4(c) indicates that the $z\nu$ value also tends to be greater than 1 below ∼1.2 K. It is generally considered that $z\nu > 1$ is a hallmark of the occurrence of QGS, thus the abrupt increase of B_c below ∼1.2 K is caused by the quenched disorder. The temperature for $z\nu = 1$ is defined as the vortex melting temperature T_M [26]. Below T_M, the quantum fluctuation dominates over the thermal fluctuation, on the other side the influence of quenched disorder on the vortices also becomes powerful. Finally, at high field [but $B \lesssim B_c(T)$] and $T < T_M$ regime, the system is transformed into a vortex glasslike phase composed of spatially separated superconducting rare regions (puddles or islands). The sizes of these rare regions increase exponentially as approaching zero temperature [53], and the slow dynamics of these large superconducting regions results in the divergency of the critical exponent $z\nu$. Recently, the high field vortex glasslike state [29] and the spatial inhomogeneity of superconducting regions [30–32] in quasi-2D NbN superconducting films have been observed experimentally, which strongly supports the scenario of the origin of QGS mentioned above.

The divergence of $z\nu$ in SIT is also observed in the ∼3.0 and ∼2.6 nm NbN films. For these two films, the critical exponent $z\nu$ vs the critical field B_c also obeys the activated scaling law $z\nu = C|B_c - B_c^*|^{-0.6}$. The values of C and B_c^* for the two films are listed in Table I. Table I also gives the normal state sheet resistance $R_\square^N$ (the sheet resistance at 10 K) and vortex melting temperature T_M for the ∼4.0, ∼3.0, and ∼2.6 nm films. One can see that the vortex melting temperature T_M decreases with decreasing $R_\square^N$. Considering that $R_\square^N$ represents the disorder degree of a 2D superconducting system, one can readily obtain that the vortex melting temperature T_M decreases with increasing disorder degree. However, the value of T_M is still as high as ∼0.8 K even for the most disordered film (the 2.6-nm-thick film).

As an example for the 2D NbN superconducting films, we give the low-temperature B-T phase diagram of the 4.0-nm-thick film in Fig. 8. In the phase diagram the superconducting onset temperature $T_c^{on}(B)$ was obtained from the $R_\square$-T curves at zero and finite magnetic fields [Fig. 3(a)], and defined as the temperature for $dR_\square/dT = 0$ near the superconducting transition region. As the temperature is lower than $T_c^{on}(B)$ under B, the film falls into the thermal fluctuation region. In this region, $R_\square(B)$ starts to decrease with decreasing temperature due to the formation of Cooper pairs and the appearance of superconducting fluctuations. It should be noted that the $T_c^{on}(B)$ and the high field $B_c(T)$ almost follow the same trajectory. Below ∼1.2 K, the trajectory represents the boundary between insulator and quantum Griffiths state. The mean-field upper critical field $B_{c2}^{MF}(T)$ is obtained according to the Ulah-Dorsey scaling theory [54]. The calculation process is identical to that used in Ref. [23]. The solid curve in Fig. 8 is the least-squares fits to the empirical formula [55], $B_{c2}^{MF}(T) = B_{c2}^{MF}(0)[1 - (T/T_{c0})^2]$. Here the zero temperature critical field $B_{c2}^{MF}(0)$ and zero field critical temperature T_{c0} are taken as 8.16 T and 5.18 K, respectively. The temperature $T_{TA}(B)$ is the characteristic temperature above which thermally assisted vortex creep governs the electrical transport of the film. The value of $T_{TA}(B)$ is obtained from the $\log_{10} R_\square$ ($\ln R_\square$) vs T^{-1} under different B plot, which would depart from the linear part below $T_{TA}(B)$ (the film gradually reaches superconducting state below $T_{TA}(B)$). When a moderate magnetic field B is applied, thermally assisted vortex creep is the dominant transport mechanism between $T_{TA}(B)$ and $T_c^{MF}(B)$, where $T_c^{MF}(B)$ is the point in the B_{c2}^{MF} vs T curve. The QGS behavior would appear below ∼1.2 K at relative high magnetic field due to the effect of the quenched disorder.

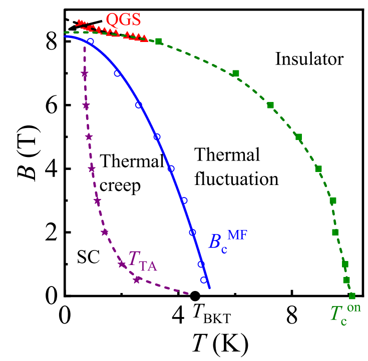

FIG. 8. B-T phase diagram of the 4.0-nm-thick NbN film. The triangles, squares, hollow circles, and stars represent the crossing field $B_c(T)$, $T_c^{on}(B)$, the mean-field critical field $B_{c2}^{MF}(T)$, and T_{TA}, respectively. The dashed curves are only the guides to eyes. The solid curve is least-squares fit to $B_{c2}^{MF}(T)/B_{c2}^{MF}(0) = 1 - (T/T_{c0})^2$. In this diagram, the regions of SC, thermal creep, and thermal fluctuation represent superconducting zone, thermally assisted vortex creep zone, and thermal fluctuation zone, respectively.

The above discussions mainly focus on the 2D NbN films. In fact, the QGS has only been reported in 2D thin films thus far. It is interesting to explore whether the phenomenon still exists when the dimensionality of the sample is increased. As mentioned above, the two ∼20-nm-thick NbN films deposited at higher nitrogen partial pressures possess lower upper critical fields and lower superconducting transition temperatures, and are quasi-3D with respect to superconductivity. We analyze the quantum phase transition in those two films below. Since the results obtained from the two films are similar, we only present and discuss the results of the film deposited at the atmosphere with 12.5% nitrogen.

Figure 9(a) shows the temperature dependence of square resistance measured at different fields. At zero field, the superconducting transition temperature is 3.86 K, which is much less than that (10.65 K) of the ∼20-nm-thick film deposited at the optimal condition. The film still reveals superconducting characteristic (i.e., the resistance drops sharply below T_c) under ∼9 T, while the characteristic completely disappears under 10 T. For the ∼20-nm-thick film deposited at the optimal conditions, it is found that the superconducting characteristic is retained even if the magnitude of the field is as large as 14 T (the maximum magnetic field for our PPMS). Figure 9(b) presents a set of magnetoresistance isotherms measured at temperatures from 0.5 to 2.8 K for the film deposited at the atmosphere with 12.5% nitrogen. Clearly, the $R_\square$-B curves do not cross at a single point or a narrow region either. At low temperatures, the crossing points of two adjacent isotherms also form a smooth curve in a relatively large and well-defined transition region around 0.6 T. These

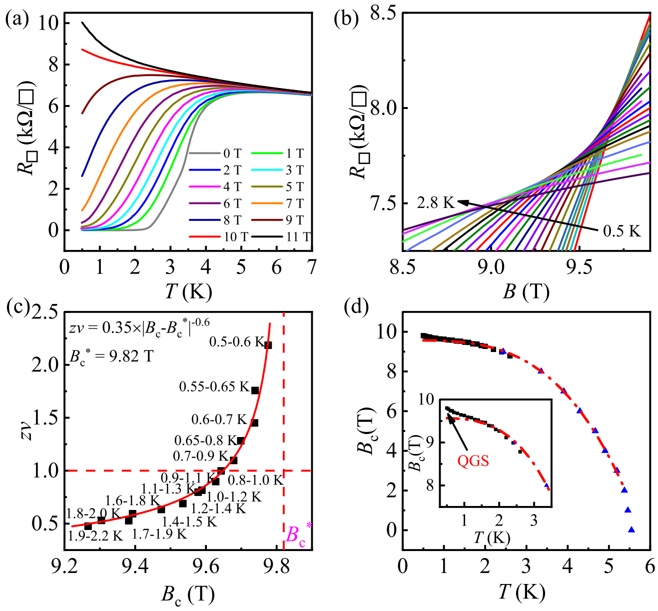

FIG. 9. (a) $R_\square(T)$ as a function of T at different fields for the 20-nm-thick NbN film deposited at the atmosphere with 12.5% nitrogen. (b) $R_\square(T)$ vs B at different temperature for the 20-nm-thick NbN film. The temperature interval between two adjacent curves is 0.05 K from 0.50 to 0.70 K, 0.10 K from 0.70 to 2.00 K, and 0.20 K for 2.00 to 2.80 K. (c) The critical field B_c dependence of critical exponent $z\nu$. (d) Temperature dependence of $T_c^{on}(B)$ (triangles) and crossing field B_c (squares). Inset: the enlarged view of (d). The dashed line is only the guide for eyes.

features are the traces for the occurrence of QGS at low temperature regime.

To check whether the film really gets into the quantum Griffiths state at low temperature and high field regime, we tentatively analyze the magnetoresistance isotherms of three adjacent temperatures using the equation $R_\square(B, \tilde{t}) = R_\square^c f[(B - B_c)\tilde{t}]$. It is found that the $R_\square(B, T)$ data for three adjacent temperatures also collapse onto two branches in the $R_\square(B, T)$ against $\delta\tilde{t}$ plot for a proper $\tilde{t}$. (In fact, the numerical calculation results of Fan and García-García indicate that a disordered superconductor driven through the 3D Anderson transition possesses some of the 2D characteristics, including strong spatial fluctuation and enhancement of the order parameter [56].) By this means, the variation of $z\nu$ with the critical field B_c of the film is obtained and plotted in Fig. 9(c). Clearly, the effective critical exponent $z\nu$ increases with increasing $B_c(T)$, becomes greater than 1.0 as $T \lesssim 1.0$ K, and tends to diverge as B_c is close to the characteristic field B_c^*. This B_c dependent behavior of $z\nu$ is very similar to that for the 2D NbN films discussed above. The $z\nu$ versus B_c data are least-squares fitted to $z\nu = C|B_c - B_c^*|^{-0.6}$, and the fitting result is drawn as the solid curve in Fig. 9(c) (the adjustable parameters C and B_c^* are given in Table I). Inspection of Fig. 9(c) indicates that the variation of $z\nu$ against $B_c(T)$ also obeys the activated scaling law for the quasi-3D NbN film. In Fig. 9(d), we gave the critical field B_c as a function of T and the magnetic field B dependence of $T_c^{on}(B)$ for the film. The $T_c^{on}(B)$ and the high field $B_c(T)$ also follow the same trajectory, which is similar to that in the 2D NbN film. Another feature of the data in Fig. 9(d) is that the value of B_c increases with decreasing temperature, and then enhance abruptly below ∼1.0 K with further decreasing temperature [see the inset of Fig. 9(d)]. The facts that the abrupt increase in B_c and $z\nu > 1$ both occur at $T \lesssim 1.0$ K strongly suggest that the quasi-3D NbN film falls into the quantum Griffiths state at high field and $T \lesssim 1.0$ K regime, as indicated by the arrow in the inset of Fig. 9(d). The QGS in the quasi-3D NbN could also originate from the quenched disorder. According to previous reports [57], the main defect in NbN films deposited at high nitrogen partial pressure is Nb vacancies, which will greatly increase the disorder level (quenched disorder) of the system. The enhanced disorder drives the system into an inhomogeneous superconducting state, consisting of domains made of phase coherent and incoherent Cooper pairs (superconducting and nonsuperconducting regions). The evolution of the superconducting and nonsuperconducting regions at low temperature and high field regime leads to the divergency of the critical exponent $z\nu$ near B_c^*. Experimentally, the disorder-induced inhomogeneity has been not only observed in 2D or quasi-2D NbN films [30–32], but also observed in homogeneously disordered quasi-3D NbN films (with thickness ∼50 nm) [58]. In fact, the emergence of inhomogeneity on the scale of the superconducting coherent length has also been observed in 3D $BaPb_{1-x}Bi_xO_3$ superconductors [59]. In addition, it has been found that the resistivity as a functions of field and temperature obeys the scaling relation of 2D superconductors, Eq. (1), as those 3D $BaPb_{1-x}Bi_xO_3$ crystals undergo field-induced superconductor to insulator transition [60]. Our work in the quasi-3D NbN film is just a beginning, and the critical behavior of 3D superconductors near the quantum phase transition deserves further investigations.

IV. CONCLUSION

Two series of epitaxial NbN films were grown on (100) MgO single crystal substrates by reactive magnetron sputtering method. The two series of films are 2D and quasi-3D, respectively, with respect to superconductivity. The low-temperature electrical transport properties of these films were systematically investigated. For the 2D films, the normal-state sheet resistance (for example, the sheet resistance at 10 K) increases with decreasing film thickness. When the normal-state sheet resistance exceeds the quantum resistance of Cooper pairs $h/4e^2$, the ground state of the films changes from superconducting to insulating state. These 2D superconducting films ($2.6 \lesssim t \gtrsim 4.0$ nm) undergo a BKT transition as transforming from normal to superconducing state upon cooling. For each 2D NbN superconducting film, a SIT can also be induced by a magnetic field perpendicular to the film plane. Upon the field-driven transition process, the intermediate anomalous metal state does not appear. However, the low-temperature magnetoresistance isotherms do not cross at a narrow range near the critical field but at a well-distinguished wide region. The dynamical critical exponent $z\nu$ tends to be divergent as $T \to 0$ and $B \to B_c^*$, which suggests the emergence of QGS behavior during the quantum phase transition. The emergence of QGS at high field and low temperature is also observed in the quasi-3D films. The QGS behavior arises from the low-temperature quenched disorder and is the consequence of the formation of the superconducting rare regions. Our results suggest that the quantum Griffiths singularity can also occur in a 2D superconductor with SIT or a quasi-3D superconductor.

ACKNOWLEDGMENTS

This work is supported by the National Natural Science Foundation of China through Grants No. 12174282 (Z.Q.L.) and No. 12074056 (P.L.).

[1] A. Hebard and M. Paalanen, Magnetic-Field-Tuned Superconductor-Insulator Transition in Two-Dimensional Films, Phys. Rev. Lett. **65**, 927 (1990).
[2] A. Yazdani and A. Kapitulnik, Superconducting-Insulating Transition in Two-Dimensional α-MoGe Thin Films, Phys. Rev. Lett. **74**, 3037 (1995).
[3] Y. Saito, Y. Kasahara, J. Ye, Y. Iwasa, and T. Nojima, Metallic ground state in an ion-gated two-dimensional superconductor, Science **350**, 409 (2015).
[4] T. I. Baturina, A. Yu. Mironov, V. M. Vinokur, M. R. Baklanov, and C. Strunk, Localized Superconductivity in the Quantum-Critical Region of the Disorder-Driven Superconductor-Insulator Transition in TiN Thin Films, Phys. Rev. Lett. **99**, 257003 (2007).
[5] N. P. Breznay, M. Tendulkar, L. Zhang, S. C. Lee, and A. Kapitulnik, Superconductor to weak-insulator transitions in disordered tantalum nitride films, Phys. Rev. B **96**, 134522 (2017).
[6] M. P. A. Fisher, Quantum Phase Transitions in Disordered Two-Dimensional Superconductors, Phys. Rev. Lett. **65**, 923 (1990).
[7] M. P. A. Fisher, P. B. Weichman, G. Grinstein, and D. S. Fisher, Boson localization and the superfluid-insulator transition, Phys. Rev. B **40**, 546 (1989).
[8] C. A. Marrache-Kikuchi, H. Aubin, A. Pourret, K. Behnia, J. Lesueur, L. Bergé, and L. Dumoulin, Thickness-tuned superconductor-insulator transitions under magnetic field in α-NbSi, Phys. Rev. B **78**, 144520 (2008).
[9] N. Marković, C. Christiansen, and A. M. Goldman, Thickness–Magnetic Field Phase Diagram at the Superconductor-Insulator Transition in 2D, Phys. Rev. Lett. **81**, 5217 (1998).
[10] N. Mason and A. Kapitulnik, Dissipation Effects on the Superconductor-Insulator Transition in 2D Superconductors, Phys. Rev. Lett. **82**, 5341 (1999).
[11] M. A. Steiner, N. P. Breznay, and A. Kapitulnik, Approach to a superconductor-to-Bose-insulator transition in disordered films, Phys. Rev. B **77**, 212501 (2008).
[12] N. P. Breznay, M. A. Steiner, S. A. Kivelson, and A. Kapitulnik, Self-duality and a Hall-insulator phase near the superconductor-to-insulator transition inindium-oxide films, Proc. Natl. Acad. Sci. USA **113**, 280 (2016).
[13] S. L. Sondhi, S. M. Girvin, J. P. Carini, and D. Shahar, Continuous quantum phase transitions, Rev. Mod. Phys. **69**, 315 (1997).
[14] D. Ephron, A. Yazdani, A. Kapitulnik, and M. R. Beasley, Observation of Quantum Dissipation in the Vortex State of a Highly Disordered Superconducting Thin Film, Phys. Rev. Lett. **76**, 1529 (1996).
[15] Y. Li, C. L. Vicente, and J. Yoon, Transport phase diagram for superconducting thin films of tantalum with homogeneous disorder, Phys. Rev. B **81**, 020505(R) (2010).
[16] A. W. Tsen, B. Hunt, Y. D. Kim, Z. J. Yuan, S. Jia, R. J. Cava, J. Hone, P. Kim, C. R. Dean, and A. N. Pasupathy, Nature of the quantum metal in a two-dimensional crystalline superconductor, Nat. Phys. **12**, 208 (2016).
[17] E. Sajadi, T. Palomaki, Z. Fei, W. Zhao, P. Bement, C. Olsen, S. Luescher, X. Xu, J. A. Folk, and D. H. Cobden, Gate-induced superconductivity in a monolayer topological insulator, Science **362**, 922 (2018).
[18] H. S. J. van der Zant, W. J. Elion, L. J. Geerligs, and J. E. Mooij, Quantum phase transitions in two dimensions: Experiments in Josephson-Junction arrays, Phys. Rev. B **54**, 10081 (1996).
[19] H. S. J. van der Zant, F. C. Fritschy, W. J. Elion, L. J. Geerligs, and J. E. Mooij, Field-Induced Superconductor-to-Insulator Transitions in Josephson-Junction Arrays, Phys. Rev. Lett. **69**, 2971 (1992).
[20] Y. Xing, H. M. Zhang, H. L. Fu, H. Liu, Y. Sun, J. P. Peng, F. Wang, X. Lin, X. C. Ma, Q. K. Xue, J. Wang, and X. C. Xie, Quantum Griffiths singularity of superconductor-metal transition in Ga thin films, Science **350**, 542 (2015).
[21] S. C. Shen, Y. Xing, P. J. Wang, H. W. Liu, H. L. Fu, Y. W. Zhang, L. He, X. C. Xie, X. Lin, J. C. Nie, and J. Wang, Observation of quantum Griffiths singularity and ferromagnetism at the superconducting $LaAlO_3/SrTiO_3(110)$ interface, Phys. Rev. B **94**, 144517 (2016).
[22] Y. Xing, K. Zhao, P. Shan, F. Zheng, Y. Zhang, H. Fu, Y. Liu, M. Tian, C. Xi, H. Liu, J. Feng, X. Lin, S. Ji, X. Chen, Q. K. Xue, and J. Wang, Ising Superconductivity and quantum phase transition in macro-size monolayer $NbSe_2$, Nano Lett. **17**, 6802 (2017).
[23] Y. Saito, T. Nojima, and Y. Iwasa, Quantum phase transitions in highly crystalline two-dimensional superconductors, Nat. Commun. **9**, 778 (2018).
[24] N. A. Lewellyn, I. M. Percher, J. Nelson, J. Garcia-Barriocanal, I. Volotsenko, A. Frydman, T. Vojta, and A. M. Goldman, Infinite-randomness fixed point of the quantum superconductor-metal transitions in amorphous thin films, Phys. Rev. B **99**, 054515 (2019).
[25] X. Zhang, A. E. Lita, H. Liu, V. B. Verma, Q. Zhou, S. W. Nam, and A. Schilling, Size dependent nature of the magnetic-field driven superconductor-to-insulator quantum-phase transitions, Commun. Phys. **4**, 100 (2021).
[26] C. Huang, E. Zhang, Y. Zhang, J. Zhang, F. Xiu, H. Liu, X. Xie, L. Ai, Y. Yang, M. Zhao, J. Qi, L. Li, S. Liu, Z. Li, R. Zhan, Y. Q. Bie, X. Kou, S. Deng, and X. C. Xie, Observation of thickness-tuned universality class in superconducting β-W thin films, Sci. Bull. **66**, 1830 (2021).
[27] X. Han, Y. Wu, H. Xiao, M. Zhang, M. Gao, Y. Liu, J. Wang, T. Hu, X. Xie, and Z. Di, Disorder-Induced Quantum Griffiths Singularity Revealed in an Artificial 2D Superconducting System, Adv. Sci. **7**, 1902849 (2020).
[28] Y. Liu, S. Qi, J. Fang, J. Sun, C. Liu, Y. Liu, J. Qi, Y. Xing, H. Liu, X. Lin, L. Wang, Q. Xue, X. Xie, and J. Wang, Observation of In-Plane Quantum Griffiths Singularity in Two-Dimensional Crystalline Superconductors, Phys. Rev. Lett. **127**, 137001 (2021).

[29] H. K. Kundu, J. Jesudasan, P. Raychaudhuri, S. Mukerjee, and A. Bid, Universal scaling behaviour near vortex-solid/glass to vortex-fluid transition in type-II superconductors in two and three dimensions, Europhys. Lett. **128**, 27001 (2019).

[30] Y. Noat, V. Cherkez, C. Brun, T. Cren, C. Carbillet, F. Debontridder, K. Ilin, M. Siegel, A. Semenov, H.-W. Hubers, and D. Roditchev, Unconventional superconductivity in ultrathin superconducting NbN flms studied by scanning tunneling spectroscopy, Phys. Rev. B **88**, 014503 (2013).

[31] C. Carbillet, V. Cherkez, M. A. Skvortsov, M. V. Feigelman, F. Debontridder, L. B. Ioffe, V.S. Stolyarov, K. Ilin, M. Siegel, D. Roditchev, T. Cren, and C. Brun, Spectroscopic evidence for strong correlations between local superconducting gap and local Altshuler-Aronov density of states suppression in ultrathin NbN films, Phys. Rev. B **102**, 024504 (2020).

[32] C. Carbillet, S. Caprara, M. Grilli, C. Brun, T. Cren, F. Debontridder, B. Vignolle, W. Tabis, D. Demaille, L. Largeau, K. Ilin, M. Siegel, D. Roditchev, and B. Leridon, Confnement of superconducting fuctuations due to emergent electronic inhomogeneities, Phys. Rev. B **93**, 144509 (2016).

[33] D. Kowal and Z. Ovadyahu, Scale dependent superconductor-insulator transition, Physica C **468**, 322 (2008).

[34] A. Möbius, Comment on "Critical behavior of the zero-temperature conductivity in compensated silicon, Si:(P, B)", Phys. Rev. B **40**, 4194 (1989).

[35] H. M. Jaeger, D. B. Haviland, B. G. Orr, and A. M. Goldman, Onset of superconductivity in ultrathin granular metal films, Phys. Rev. B **40**, 182 (1989).

[36] M. P. A. Fisher, G. Grinstein, and S. M. Girvin, Presence of Quantum Diffusion in two Dimensions: Universal Resistance at the Superconductor-Insulator Transition, Phys. Rev. Lett. **64**, 587 (1990).

[37] R. Koushik, S. Kumar, K. R. Amin, M. Mondal, J. Jesudasan, A. Bid, P. Raychaudhuri, and A. Ghosh, Correlated Conductance Fluctuations Close to the Berezinskii-Kosterlitz-Thouless Transition in Ultrathin NbN Films, Phys. Rev. Lett. **111**, 197001 (2013).

[38] M. Mondal, M. Chand, A. Kamlapure, J. Jesudasan, V. C. Bagwe, S. Kumar, G. Saraswat, V. Tripathi, and P. Raychaudhuri, Phase Diagram and Upper Critical Field of Homogeneously Disordered Epitaxial 3-Dimensional NbN Films, J. Supercond. Nov. Magn. **24**, 341 (2011).

[39] V. L. Berezinskii, Destruction of long-range order in one-dimensional and two-dimensional systems possessing a continuous symmetry group. II. quantum systems, Sov. Phys. JETP **34**, 610 (1972).

[40] J. M. Kosterlitz and D. J. Thouless, Long range order and metastability in two dimensional solids and superfluids.(Application of dislocation theory), J. Phys. C: Solid State Phys. **5**, L124 (1972).

[41] J. M. Kosterlitz and D. J. Thouless, Ordering metastability and phase transitions in two-dimensional systems, J. Phys. C **6**, 1181 (1973).

[42] S. A. Wolf, D. U. Gubser, W. W. Fuller, J. C. Garland, and R. S. Newrock, Two-Dimensional Phase Transition in Granular NbN Films, Phys. Rev. Lett. **47**, 1071 (1981).

[43] R. C. Dynes, J. P. Garno, and J. M. Rowell, Two-Dimensional Electrical Conductivity in Quench-Condensed Metal Films, Phys. Rev. Lett. **40**, 479 (1978).

[44] Z. Ovadyahu, Transition to Zero Vorticity in a Two-Dimensional Superconductor, Phys. Rev. Lett. **45**, 375 (1980).

[45] K. Epstein, A. M. Goldman, and A. M. Kadin, Vortex-Antivortex Pair Dissociation in Two-Dimensional Superconductors, Phys. Rev. Lett. **47**, 534 (1981).

[46] A. F. Hebard and A. T. Fiory, Evidence for the Kosterlitz-Thouless transition in thin superconducting aluminum films, Phys. Rev. Lett. **44**, 291 (1980).

[47] R. F. Voss, C. M. Knoedler, and P. M. Horn, Phase-Slip Shot Noise at the Two-Dimensional Superconducting Transition: Evidence for Vortices? Phys. Rev. Lett. **45**, 1523 (1980).

[48] B. I. Halperin and D. R. Nelson, Resistive transition in superconducting films, J. Low Temp. Phys. **36**, 599 (1979).

[49] A. M. Kadin, K. Epstein, and A. M. Goldman, Renormalization and the Kosterlitz-Thouless transition in a two-dimensional superconductor, Phys. Rev. B **27**, 6691 (1983).

[50] M. V. Feigel'man, V. B. Geshkenbein, and A. I. Larkin, Pinning and creep in layered superconductors, Physica C **167**, 177 (1990).

[51] T. Vojta, A. Farquhar, and J. Mast, Infinite-randomness critical point in the two-dimensional disordered contact process, Phys. Rev. E **79**, 011111 (2009).

[52] A. Del Maestro, B. Rosenow, J. A. Hoyos, and T. Vojta, Dynamical Conductivity at the Dirty Superconductor-Metal Quantum Phase Transition, Phys. Rev. Lett. **105**, 145702 (2010).

[53] T. Vojta, C. Kotabage, and J. A. Hoyos, Infinite-randomness quantum critical points induced by dissipation, Phys. Rev. B **79**, 024401 (2009).

[54] S. Ullah and A. T. Dorsey, Critical Fluctuations in High-Temperature Superconductors and the Ettingshausen Effect, Phys. Rev. Lett. **65**, 2066 (1990).

[55] N. W. Ashcroft and N. D. Mermin, *Solid State Physics* (Holt Rinehart and Winston, New York, 1976), p. 745.

[56] B. Fan and A. M. García-García, Superconductivity at the three-dimensional Anderson metal-insulator transition, Phys. Rev. B **102**, 184507 (2020).

[57] S. P. Chockalingam, M. Chand, J. Jesudasan, V. Tripathi, and P. Raychaudhuri, Superconducting properties and Hall effect of epitaxial NbN thin films, Phys. Rev. B **77**, 214503 (2008).

[58] A. Kamlapure, T. Das, S. C. Ganguli, J. B. Parmar, S. Bhattacharyya, and P. Raychaudhuri, Emergence of nanoscale inhomogeneity in the superconducting state of a homogeneously disordered conventional superconductor, Sci. Rep. **3**, 2979 (2013).

[59] C. Parra, F. C. Niestemski, A. W. Contryman, P. Giraldo-Gallo, T. H. Geballe, I. R. Fisher, and H. C. Manoharan, Signatures of two-dimensional superconductivity emerging within a three-dimensional host superconductor, Proc. Natl. Acad. Sci. USA **118**, e2017810118 (2021).

[60] P. Giraldo-Gallo, H. Lee, Y. Zhang, M. J. Kramer, M. R. Beasley, T. H. Geballe, and I. R. Fisher, Field-tuned superconductor-insulator transition in $BaPb_{1-x}Bi_xO_3$, Phys. Rev. B **85**, 174503 (2012).